Journal of Astronomical Telescopes, Instruments, and Systems

AstronomicalTelescopes.SPIEDigitalLibrary.org

SpUpNIC (Spectrograph Upgrade: Newly Improved Cassegrain): a versatile and efficient low- to medium-resolution, long-slit spectrograph on the South African Astronomical Observatory's 1.9-m telescope

Lisa A. Crause
David Gilbank
Carel van Gend
Hannah L. Worters
Craig Sass
Enrico J. Kotze
Stephen Potter
Amanda Sickafoose
Ramotholo Sefako
John Southworth
Lucas Macri
John Thorstensen
Cezary Galan
Patricia Skelton
Chris Engelbrecht
Ian Braker
Hartmut Winkler
Daniel Pieńkowski
Derya Sürgit
Ahmet Erdem
Matt Burleigh

Lisa A. Crause, David Gilbank, Carel van Gend, Hannah L. Worters, Craig Sass, Enrico J. Kotze, Stephen Potter, Amanda Sickafoose, Ramotholo Sefako, John Southworth, Lucas Macri, John Thorstensen, Cezary Galan, Patricia Skelton, Chris Engelbrecht, Ian Braker, Hartmut Winkler, Daniel Pieńkowski, Derya Sürgit, Ahmet Erdem, Matt Burleigh, "SpUpNIC (Spectrograph Upgrade: Newly Improved Cassegrain): a versatile and efficient low- to medium-resolution, long-slit spectrograph on the South African Astronomical Observatory's 1.9-m telescope," *J. Astron. Telesc. Instrum. Syst.* **5**(2), 024007 (2019), doi: 10.1117/1.JATIS.5.2.024007.

SpUpNIC (Spectrograph Upgrade: Newly Improved Cassegrain): a versatile and efficient low- to medium-resolution, long-slit spectrograph on the South African Astronomical Observatory's 1.9-m telescope

Lisa A. Crause,[a,*] David Gilbank,[a] Carel van Gend,[a] Hannah L. Worters,[a] Craig Sass,[a] Enrico J. Kotze,[a] Stephen Potter,[a] Amanda Sickafoose,[a,b] Ramotholo Sefako,[a] John Southworth,[c] Lucas Macri,[d] John Thorstensen,[e] Cezary Galan,[f] Patricia Skelton,[g] Chris Engelbrecht,[h] Ian Braker,[i] Hartmut Winkler,[h] Daniel Pieńkowski,[j] Derya Sürgit,[k,l] Ahmet Erdem,[k,m] and Matt Burleigh[i]

[a]South African Astronomical Observatory, Cape Town, South Africa
[b]Massachusetts Institute of Technology, Cambridge, Massachusetts, United States
[c]Keele University, Staffordshire, United Kingdom
[d]Texas A&M University, College Station, Texas, United States
[e]Dartmouth College, Hanover, New Hampshire, United States
[f]Nicholas Copernicus Astronomical Center, Warsaw, Poland
[g]University of South Africa, Pretoria, South Africa
[h]University of Johannesburg, Department of Physics, Johannesburg, South Africa
[i]University of Leicester, Department of Physics and Astronomy, Leicester, United Kingdom
[j]Warsaw University Observatory, Warszawa, Poland
[k]Astrophysics Research Centre and Observatory, Çanakkale, Turkey
[l]Çanakkale Onsekiz Mart University, Department of Space Sciences and Technologies, Faculty of Arts and Sciences, Çanakkale, Turkey
[m]Çanakkale Onsekiz Mart University, Department of Physics, Faculty of Arts and Sciences, Çanakkale, Turkey

Abstract. We report on the extensively upgraded Cassegrain spectrograph on the South African Astronomical Observatory (SAAO) 1.9-m telescope. The introduction of new collimator and camera optics, a new detector and controller, a rear-of-slit viewing camera to facilitate acquisition, and a new instrument control and quick-look data-reduction software (to take advantage of the entire system now being governed by a programmable logic controller) has revolutionized this workhorse instrument on Africa's second largest optical telescope. The improvement in throughput over the previous incarnation of the spectrograph is ~50% in the red, increasing to a factor of four at the blue end. A selection of 10 surface-relief diffraction gratings is available to users, offering a variety of wavelength ranges and resolutions, with resolving powers between ~500 and 6500. SpUpNIC (Spectrograph Upgrade: Newly Improved Cassegrain) has been scheduled for ~80% of the time available on the 1.9-m since being installed on the telescope in late October 2015, providing the single-object spectroscopic capability to support the broad research interests of the SAAO's local and international user community. We present an assortment of data obtained for various observing programs to demonstrate different aspects of the instrument's enhanced performance following this comprehensive upgrade. [DOI: 10.1117/1.JATIS.5.2.024007]

Keywords: spectrograph; Cassegrain; SpUpNIC; South African Astronomical Observatory; instrumentation.

Paper 18079 received Sep. 30, 2018; accepted for publication Apr. 23, 2019; published online May 14, 2019.

1 Introduction

The main instrument for the South African Astronomical Observatory (SAAO) 1.9-m[1] telescope has long been a Cassegrain spectrograph. A number of upgrades have taken place over the four decades that the instrument has been in use, and most have centered on replacing the detector system to keep pace with technological advances. The earliest version included a photographic plate that was fed by an image intensifier. This was later replaced by a photon-counting system, which gave way to a pair of linear photodiode arrays. In 1997, the introduction of a charge-coupled device (CCD) was seen, and a few years later, it was decided that the spectrograph's inefficient Maksutov–Cassegrain camera optics would be replaced with a more elegant folded-Schmidt design to increase the throughput of the instrument.

The spectrograph upgrade project received intermittent attention while observatory efforts were focused on the Southern African Large Telescope (SALT). A programmable logic controller (PLC) system was introduced in 2009 to enable most of the moving components (stepper motors and pneumatic actuators) and on/off toggles for lamps within the spectrograph to be placed under software control. This simplified the operation of the instrument, but the daily focusing of the camera optics remained a time-consuming manual task. In October 2014, the old spectrograph (informally known as Cassie, or the SpCCD) was taken out of service to allow completion of the upgrade. By then, the scope of the project had increased considerably, to the point that it would effectively yield a new spectrograph (see Fig. 1), although including some original components, such as the slit mechanism.

*Address all correspondence to Lisa A. Crause, E-mail: lisa@saao.ac.za

2329-4124/2019/$25.00

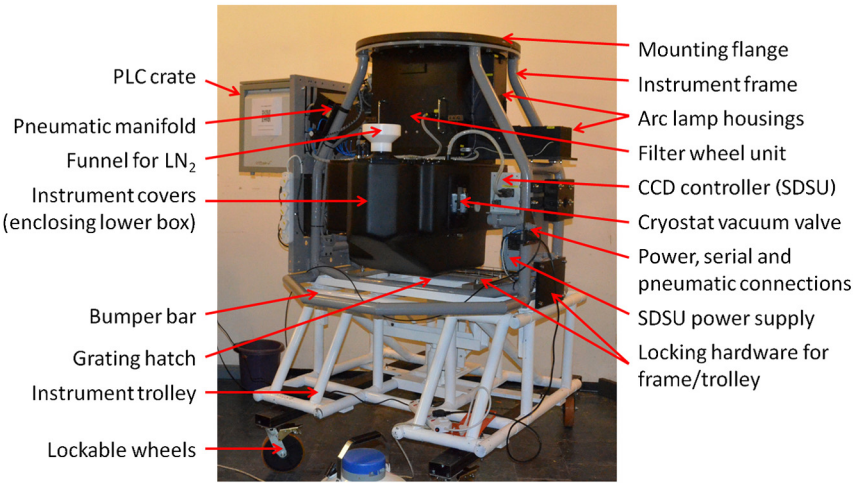

Fig. 1 External layout of SpUpNIC.

Along with the modern CCD, all new camera and collimator optics and new software came with the ability to automate the spectrograph camera focus routine since the camera's spherical primary mirror was also motorized. A rear-of-slit viewing system was also incorporated to improve the acquisition and telescope-focusing processes for the instrument. User-friendly Python-based software was developed [both for the back end, operating at the driver level, and for the graphical user interfaces (GUIs) responsible for instrument control and quick-look data reduction] to render the spectrograph vastly more efficient to operate. The use of color on the instrument control GUI highlights when the system is not appropriately configured for science exposures. This saves time that might otherwise be wasted by observing a target with mechanisms related to acquisition or calibration inadvertently left in the beam.

The technical details of the modified instrument, Spectrograph Upgrade: Newly Improved Cassegrain (SpUpNIC),[2] were presented at the 2016 SPIE Astronomical Telescopes and Instrumentation conference, and this paper focuses on operational aspects and scientific performance.

2 Instrument Description

2.1 *Optics*

This upgrade was driven by new spectrograph-camera optics. A folded-Schmidt design replaced the Maksutov–Cassegrain camera, the central obscuration of which blocked more than half of the light. In the new system, much of the slot in the camera's fold-mirror is hidden within the obscuration produced by the inverse-Cassegrain collimator, which itself lies within the shadow of the telescope secondary. The SpUpNIC optical layout is shown in Fig. 2(a), and the CAD model of the optomechanical assembly is shown in Fig. 2(b), along with the liquid nitrogen tank for cooling the CCD.

Dispersed light leaving the surface-relief diffraction grating passes through a Schmidt plate before striking the slotted fold-mirror. The fold-flat directs the beam to the spherical primary mirror, which focuses the light (through the slot in the fold-mirror) onto the CCD, after passing through the field-flattener lens that forms the cryostat window. The spectrograph focus is adjusted by means of a stepper motor connected to the camera's

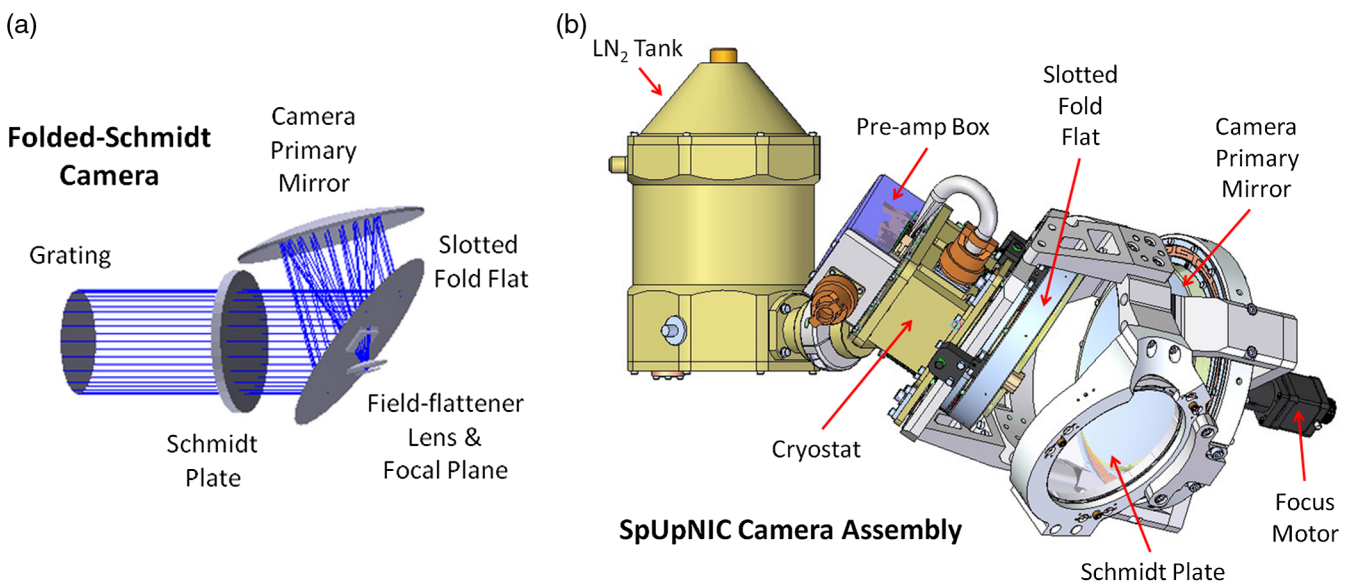

Fig. 2 (a) Optical layout of the SpUpNIC camera and (b) the CAD model for the new camera assembly.

Table 1 Characteristics of the SpUpNIC diffraction gratings. Resolving powers are derived from mean FWHM of arc lines measured across the full spectrum, and then calculated at the blaze wavelength. For G10–G13, which are typically used significantly blueward of their blaze wavelengths, the resolving powers are overestimated by 15%–20%.

Name	Lines/mm	Blaze (Å)	Wavelength range (Å)	Dispersion (Å/pixel)	Resolving power
G4	1200	5100	1250	0.62	3000
G5	1200	6200	1100	0.53	3100
G6	600	5100	2800	1.4	1000
G7	300	5000	5500	2.7	500
G8	400	8500	4100	2.2	1200
G9	830	7800	1750	0.84	2400
G10	1200	10,000	950	0.47	6500
G11	600	10,000	2600	1.3	1300
G12	300	10,000	5600	2.8	1000
G13	2160	5000	550	0.27	4100

concave primary mirror. This mirror is mounted to a pair of wire-cut, annular flexures made of beryllium-copper, which ensures pure axial translation over the full focus range.

The $F/2.2$ inverse-Cassegrain collimator was also replaced, with an $F/1.4$ version that yields a larger collimated beam. This was necessary to reduce the fractional light-loss due to the slot in the camera's fold-mirror. A new planoconvex field lens with the required focal length was placed just below the slit to accommodate the resulting changes to the optical system.

The spectrograph still uses the same set of surface-relief diffraction gratings that were employed previously, although those that had suffered operational abuse were replaced. Furthermore, a new grating (G13) with 2160 lines/mm and blazed at 5000 Å has been added to the collection to provide higher resolving power in the blue that was available in the past. The properties of the 10 gratings are listed in Table 1. Two different arc lamps (CuAr and CuNe) for wavelength calibration can either be used individually or simultaneously. G5 requires the CuNe lamp, whereas the CuAr lamp is suitable for all of the other gratings.

2.2 *Detector*

The SAAO was to be deeply involved in the spectroscopic follow-up of the Edinburgh-Cape Blue Object Survey[3] at the time that the spectrograph upgrade was initially planned (in the late 1990s). This provided significant motivation for selecting a blue-sensitive CCD and so an E2V CCD42-10 chip was purchased. It has 13.5-μm pixels arranged in a 2048×512 array and is thinned and back-illuminated, with a broadband antireflection coating that results in the detector quantum efficiency peaking in the blue/green (see Table 2). One half of the chip is masked off and pseudoframe transfer readout is implemented, so only half of the vertical extent of the 27.6 mm $\times$ 6.9 mm imaging area is used. This corresponds to the slit spatially sampling 120 arc sec on the sky.

Table 2 SpUpNIC detector quantum-efficiency values provided by the manufacturer, E2V.

Wavelength (Å)	3500	5000	6500	9000
Quantum efficiency (%)	50	85	70	35

Table 3 SpUpNIC detector readout mode characteristics (1×2 binned). The readout times for 1×1 binned images are approximately double those listed below.

CCD mode	Gain (e^-/ADU)	Read-noise (e^-RMS)	Readout (s)
Faint/slow	1.15	2.57	4.1
Bright/fast	5.55	6.68	2.4
Faint/fast	2.06	15.8	2.4
Bright/slow	2.80	2.53	4.1

The CCD has an extremely low noise amplifier and the chip is usually 1×2 binned (in the spatial direction) to increase the signal-to-noise (S/N) ratio. Thermal/electronic noise is minimized by cooling the CCD to -105°C with liquid nitrogen. The system has four modes offering different gain/readout-speed combinations (see Table 3), but in practice, only the faint/slow mode tends to be used as it allows faint targets to utilize the full dynamic range of the analog-to-digital converter. The bright/fast mode is more suitable for bright targets that require most of the pixels' full well depth to avoid saturation. The CCD shows no sign of nonlinearity below 50,000 counts/pixel. SpUpNIC employs the SDSU Generation III CCD controller architecture.

2.3 *Rear-of-Slit Camera*

A key addition to the upgraded spectrograph is a rear-of-slit camera that facilitates the acquisition process, by allowing users to directly view the star going down the slit. One can also focus the telescope more efficiently with feedback provided by this image of the star. Astigmatism in the system conveniently causes the star to elongate diagonally (top left to bottom right and vice versa) on either side of the best focus.

The system is operated by deploying a small, pneumatically actuated fold-mirror into the beam (between the two collimator mirrors) in order to view the slit from below. A stand-alone GUI was developed in-house to control the compact USB2.0 Starlight Xpress Lodestar CCD camera and the image display can be adjusted while exposures are running to optimize the view. Depending on sky conditions, it is possible to acquire targets as faint as $V \sim 17$ with this system. Fainter targets have to be positioned on the slit using a more indirect method that uses the acquisition camera associated with the telescope control system (TCS), as was done with earlier versions of the spectrograph.

A further advantage of being able to view the slit from below is that one can easily check that a target is still properly positioned, without having to relinquish the guide star. This is particularly useful when taking a long series of exposures of the same object.

2.4 *Software*

The new spectrograph software follows a distributed architecture, with drivers for individual hardware components, namely the PLC and the detector system, implemented as stand-alone server processes. These are connected to corresponding clients over TCP/IP sockets. The clients are bundled together and instantiated by a controller class, on top of which is a user interface implemented in Python using the Qt widget set.

The PLC places all mechanisms and toggles under software control. Thus, it is possible to adjust the slit width, grating angle, and spectrograph camera focus directly from the GUI, rather than having to manually set those positions on the instrument (as was necessary prior to the upgrade). The pneumatic actuators for the rear-of-slit mirror and the Hartmann shutter, as well as the toggles for the arc lamps and the slit illumination, are also controlled via the GUI. Therefore, it is possible to configure the instrument for a given type of exposure or to execute a focus sequence (which used to be a tedious, iterative manual process) with the click of a button.

The instrument control GUI (shown in Fig. 3) includes an interactive schematic representation of the instrument that may be used to configure the system, either for acquisition, calibration, or target observations. This intuitive interface streamlines the observing process, and the use of colored highlights on certain indicators and on the frame around the schematic warn that the system is not configured for a science observation, i.e., the absence of color indicates readiness for a science exposure. This saves time that was easily wasted previously when users would forget to remove a mirror from the beam or switch off a lamp before taking a science frame.

SpUpNIC also has a new quick-look data reduction GUI that displays the 2-D images and produces extracted, sky-subtracted, wavelength-calibrated 1-D spectra as soon as an image is saved at the end of an exposure (see Fig. 4). Extraction and sky subtraction regions, smoothing and display options can be changed on-the-fly and the output is automatically saved as an IRAF[4]-compatible multispec FITS file, as well as a simple text file suitable for plotting.

The large number of gratings available (10) and the broad range of angles that each of them can be used at makes providing guaranteed science-quality wavelength solutions impractical. The accuracy of the wavelength calibration is therefore appropriate for the spirit of a quick-look tool, typically ~2 Å. This allows observers to confirm that the wavelength range of interest is being covered and to identify spectral features in science frames. It is not intended to be a final science-quality level reduction, although, for some users, this may be sufficient for their science requirements. Even if the wavelength calibration is not precise enough, the quick-look output can serve as a useful starting point for more rigorous data reduction.

Having loaded an arc frame, the quick-look applies that wavelength solution to the next object frame and displays it. The automatic extraction chooses the highest peak, or the most central peak, in the image, around which a region is extracted (shaded green in Fig. 5). Alternatively, the extraction region can be manually defined. The default sky-subtraction regions (shaded red) are above and below the extraction band, and either or both of those can be used, or sky-subtraction can be deselected. The sky subtraction regions can also be adjusted to avoid other objects that may fall on the slit. The quick-look's 2-D and 1-D plots can be interrogated further by zooming and panning within the

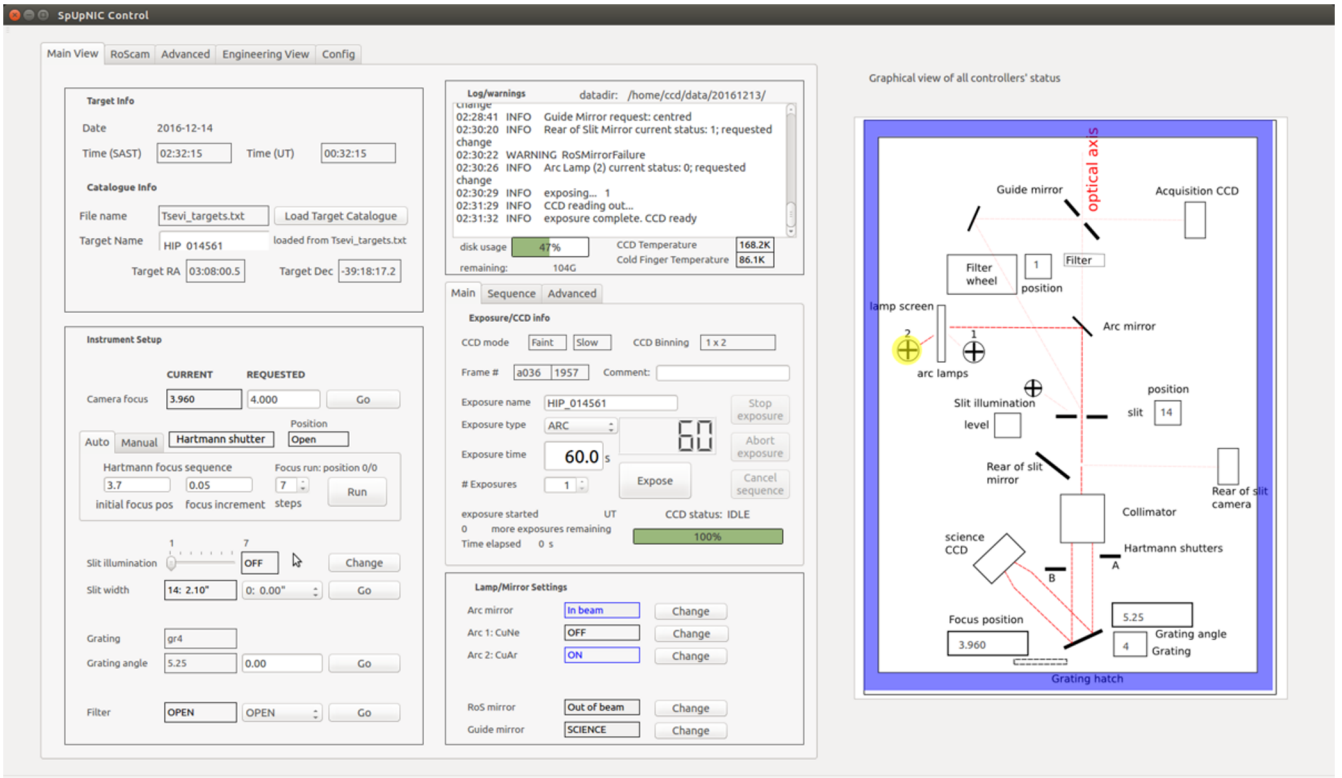

Fig. 3 Screenshot of the SpUpNIC Control GUI, showing the interactive schematic on the right. The blue frame around the schematic signifies that the system is not configured for a science frame. The light path, indicated in red, shows that the instrument is set up for an arc exposure in this case.

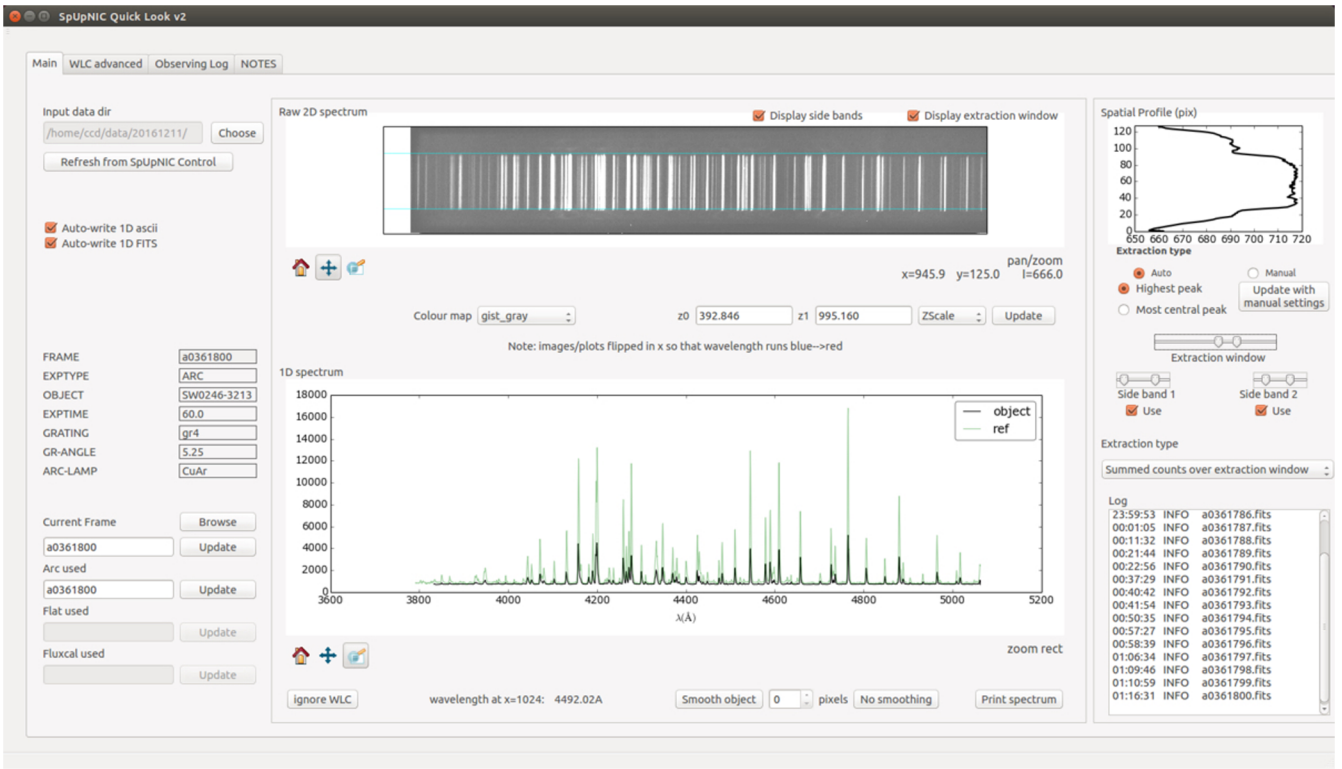

Fig. 4 Screenshot of the SpUpNIC quick-look GUI, displaying a CuAr arc frame. A row is extracted from the center of the 2-D image and plotted as a 1-D spectrum. The arc lines (shown in black) are matched to a template arc (shown in green) in order to apply an approximate wavelength calibration.

Fig. 5 Screenshot of the SpUpNIC quick-look GUI, displaying an object spectrum that has been extracted, sky-subtracted and approximately wavelength calibrated.

respective displays. The quick-look does not currently apply bias correction, flat-fielding, or cosmic ray rejection.

3 Operation

Wikis were selected as an easily accessible and editable platform to host current instrument documentation at the SAAO. Detailed up-to-date information about the spectrograph is therefore provided on the observatory's SpUpNIC wiki page. The change log section near the top of the wiki highlights significant revisions made to the system, and subsequent sections provide instructions for getting the instrument set up, obtaining calibration data, carrying out observations, and addressing known issues that crop up periodically.

3.1 *Grating Setup*

The sample arcs shown in Fig. 6 give a visual indication of the wavelength ranges and dispersions offered by the instrument's 10 different gratings. The old grating names have been retained for continuity and so, the numbering scheme runs from G4–G13. G10, G11, and G12 (all blazed at 10,000 Å) are the red equivalents of G5, G6, and G7, whereas G7, G6, G4, and G13, all blazed near 5000 Å, provide increasing resolving powers between $R \approx 500$ and $R \approx 4000$.

The GG 495 order-blocking filter is required for several of the gratings, and certain arc filters are needed to prevent saturation by extremely bright lines in the red. Each grating holder is magnetically encoded so that the PLC can identify it, and hence, the control-software automatically selects and inserts the appropriate filter into the beam. The BG 38 and GG 495 arc filters, mounted in old brass holders, have to be manually inserted into the relevant arc lamp filter slots on the instrument, depending on the grating in use.

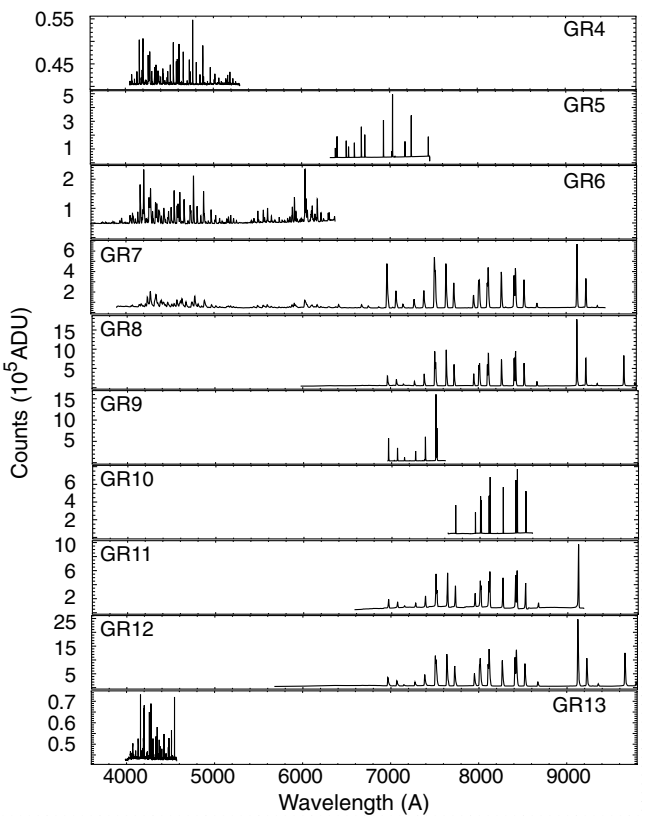

Fig. 6 Sample arc spectra obtained with each of the SpUpNIC gratings to give an indication of their wavelength ranges and relative dispersions. Adjusting the grating angle shifts the spectrum in wavelength, so these plots do not convey the full spectral coverage provided by all of the gratings.

G5 is the only grating that requires the CuNe lamp in order to obtain enough lines for a good wavelength solution, all the other gratings use the CuAr lamp. Both lamps are permanently available on SpUpNIC (previously, users had to physically swap lamps when changing gratings), and it is possible to employ both lamps simultaneously. Users need to change gratings manually, a detailed procedure for which is provided on the wiki.

3.2 *Hartmann Focus Routine*

The PLC enables the automation of time-consuming procedures like focusing the spectrograph camera. This is typically performed daily and whenever a grating change is done. The control GUI allows the user to set the starting value, step size, and number of steps for a focus run. Once the system is configured for an arc exposure (the arc mirror in the beam and the required arc lamp on), clicking the Hartmann sequence Run button launches the focus routine.

During this process, the slit width is automatically reduced to yield sharp lines and the focus setting is changed after each pair of images. These pairs of arc frames are taken with a pneumatically driven shutter blocking one half of the beam and then the other. The individual images in each pair are then cross-correlated to determine their relative shift and best focus is where the shift is minimized. At the end of the sequence, the appropriate focus value is automatically sent to the PLC (which commands the camera primary mirror to the required axial position), and the slit width is returned to its prefocus run position. Progress during the execution of the focus routine can be followed on the quick-look GUI, which displays the various arcs and calculated shifts for each pair, as well as the estimated best-focus value (Fig. 7).

3.3 *Target Acquisition*

The observer needs to prepare a target catalog text file containing the object names, co-ordinates, and equinox for all the objects to be observed. This file is used to populate the fits headers with target information, and it allows the co-ordinates to be sent to both the finder-chart-generation tool and then to the TCS in order to point the telescope. The catalog file is transferred directly onto the instrument PC and needs to be reloaded into the control GUI before any changes will reflect.

Acquiring a target involves three main steps. The first requires the acquisition/guide mirror to be in the beam, to direct the light to the acquisition camera on the TCS. At the start of the run, the user needs to mark the slit position on the TCS acquisition image to indicate where targets need to be approximately positioned. One then centers the acquisition mirror and places the rear-of-slit mirror in the beam, to direct the light to the rear-of-slit camera. After carefully placing the object on the slit, the final step is to select a suitable guide star from the relevant finder chart.

3.4 *Observing Sequences*

Some degree of flexure is inevitable for a large (>400 kg) Cassegrain instrument (see Sec. 5.1), therefore, we recommend

Fig. 7 Quick-look GUI during the course of a Hartmann focus sequence. The main plot shows the A and B frames for a given focus setting, along with the best-fit shift between the two. The plot in the upper right shows the measured shift as a function of focus. Best focus is where the shift is zero.

that target exposures be bracketed with arc frames that can be interpolated when performing the final wavelength calibration. If taking a series of spectra of a single object, arcs should be obtained approximately every 20 min. For convenience, there is a sequence tab on the exposure/CCD info pane of the control GUI, to automate repeat observations (including the necessary arcs). An audible signal to mark the end of each exposure, and readout, can be toggled via a check-box on the advanced tab of the exposure/CCD info pane.

3.5 *Quick-Look Extractions*

Having set the extraction window, one can check for saturation (which occurs around 65k counts/pixel) using the "peak-counts" extraction option. This only plots the row across the spectrum that contains the highest number of counts. Once satisfied with the exposure, the "summed counts" option yields the full extraction, which are the data saved as the quick-look spectrum. Sky-subtraction may be included, and the user can define the position(s) of those regions manually or automatically.

The spectrum can also be smoothed by a user-defined number of pixels, and the wavelength solution derived from the arc loaded most recently can be ignored if one wishes to see the display in pixels instead of Angstroms. There is an extra tab on the quick-look GUI to allow the user to tweak the wavelength solution if, for some reason, the latest arc (black in Fig. 4) is not well matched to the library arc (green in Fig. 4).

3.6 *Data Storage and Transfer*

Every SpUpNIC frame readout is saved to a FITS file. These are stored in nightly directories on the SpUpNIC computer in the 1.9-m control room. The following morning, the data are transferred and stored on a Sutherland server, from where they are then transferred and stored on a Cape Town server. An additional copy of the raw data is also saved to the Sutherland server.

The individual raw FITS files are 544 kB in size, whereas the quick-look's IRAF-compatible multispec files are 44 kB and the 1-D text files, also produced by the quick-look software, are 208 kB. All of the quick-look products are saved in a subdirectory in each nightly directory.

A sample FITS header, which includes detailed information about the instrument configuration, telescope pointing, and environmental conditions, is shown in Fig. 8. The quick-look also uses the FITS headers to automatically generate an observing log that contains relevant information about the individual files. This log is produced for all the FITS files in the quick-look's working directory and can be exported as a text file.

4 Performance

4.1 *Throughput Improvement*

The increase in spectrograph throughput was quantified by observing the same spectrophotometric standard stars (under photometric conditions) using the old spectrograph (aka Cassie) in October 2014 and SpUpNIC in October 2015. The slight reduction in the dispersion and the difference in CCD gains between the old and new system had to be accounted for before the pairs of spectra could be compared directly, as shown in Fig. 9. The lowest resolution grating (G7) most clearly illustrates the dramatic increase in performance, particularly toward the blue end of the spectrum. Here, the combination of the improved CCD quantum-efficiency and the throughput doubling

```
SIMPLE  =                    T / conforms to FITS standard
BITPIX  =                   16 / array data type
NAXIS   =                    2 / number of array dimensions
NAXIS1  =                 2148
NAXIS2  =                  128
EXTEND  =                    T
BSCALE  =                    1
BZERO   =                32768
UT-START= '17:19:23'            / UT time (start)
LC-START= '19:19:23'            / local time (start)
DATE-OBS= '2017-07-29'          / UT date (start)
HJD-OBS =    57964.22179870979 / Heliocentric Julian Date (start)
EXPOSURE=                 30.0 / Total exposure time
HBIN    =                    2 / Horizontal binning
VBIN    =                    1 / Vertical binning
GAINVAL =                1.145 / Gain value
NOISEADU=                2.245 / Noise (ADU)
NOISEEL =                 2.57 / Noise (electrons)
TELRA   = '14:11:44'            / The telescope right ascension
TELDEC  = '-33:02:28'           / The telescope declination
AIRMASS = '1.0247  '            / The airmass (sec(z))
ZD      = '0.220009463757'      / The telescope zenith distance
HA      = '1:00:56 '            / The telescope hour angle
TELFOCUS= '2213    '            / The telescope focus
INSTANGL= '90      '            / The instrument angle
DOMEPOS = '61.8    '            / The dome position
TMTDEW  = '18.24   '            / Difference between current and dew-point temps
HUMIDIT = '27.89   '            / The average humidity
RELSKYT = '39.59   '            / The relative sky temperature (avg cloud cover)
WIND    = '20.69   '            / The average wind speed
ENVTEM  = '12.37   '            / The average ambient temperature
SEEING  = '1.0     '            / The curent seeing
OBSERVER= 'Crause  '            / OBSERVER NAME
RUN-NO  = '056     '            / RUN NUMBER
GRATING = 'gr13    '            / GRATING NAME
GR-ANGLE= '-8.00   '            / GRATING ANGLE
SLITPOS = '8       '            / SLIT WIDTH (index)
SLITWID = '1.20    '            / SLIT WIDTH (arcsec)
FILTER  = 'OPEN    '            / FILTER NAME
FRAME   = '1496    '            / FRAME NUMBER
OBJECT  = 'CD_-32_9927'         / Target name
EXPTIME = '30.0    '            / ACTUAL EXPOSURE TIME (s)
EXPTYPE = 'ARC     '            / EXPOSURE TYPE
BINNING = '1x2     '            / CCD binning
CCDSUM  = '1 2     '            / CCD binning
SGAIN   = 'Faint   '            / CCD Mode GAIN
SRDNOISE= 'Slow    '            / CCD Mode RDNOISE
CCDTEMP = '168.1K  '            / CCD temperature
CF-TEMP = '85.1K   '            / Cold Finger Temperature
ARC-LAMP= 'CuAr    '            / arc lamp ID
FOCUSPOS=               4.1399 / Focus position (mm)
HARTPOS = 'Open    '            / Position of Hartmann Shutter
TARG-RA = '14:11:46.4'
TARG-DEC= '-33:03:14'
HARTSEQ = '0/0     '            / Position in Hartmann sequence
COMMENT Testing G13
END
```

Fig. 8 Sample FITS header for a SpUpNIC arc frame.

due to the new camera optics yields a fourfold increase. The lower red sensitivity of the new detector reduces the overall system improvement to a factor of ∼1.5 at longer wavelengths.

Various users have also verified these results when reobserving targets with the new instrument. For the popular blue grating (G4), slightly higher S/N spectra are obtained with four times shorter exposures than were required previously (see Fig. 10).

The improved blue throughput is particularly useful for studying white dwarfs (WDs). Although many have been classified in the northern hemisphere due to surveys such as SDSS,[5] the number known in the southern hemisphere is much lower.

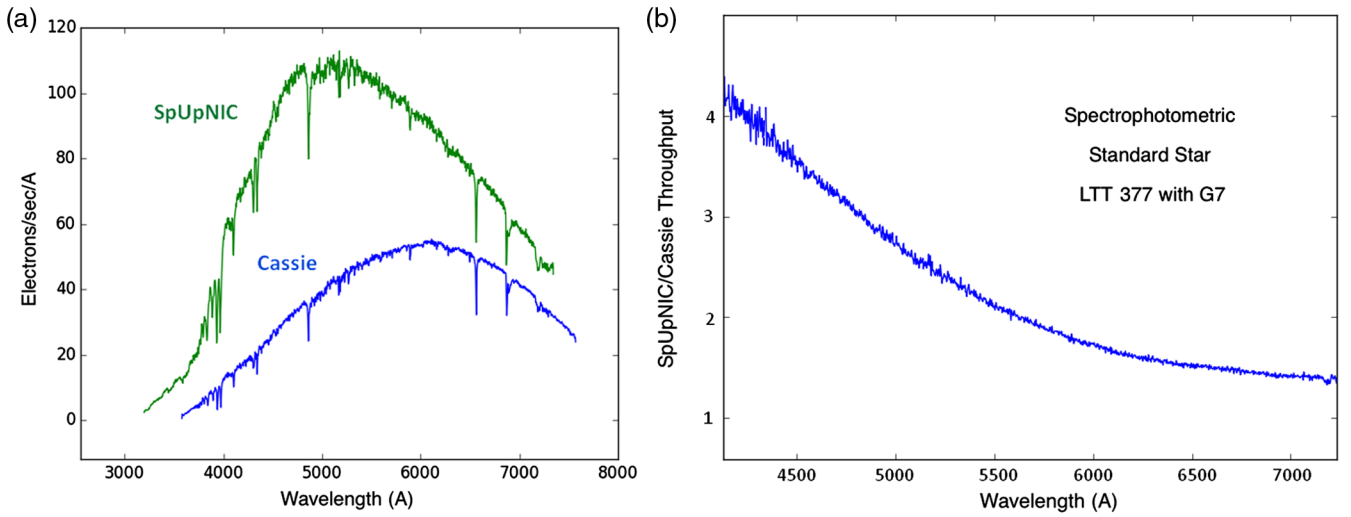

Fig. 9 (a) G7 spectra of the $V = 11.2$ sdK spectrophotometric standard star LTT 377 obtained with SpUpNIC (green) and Cassie (blue) demonstrate the considerable increase in throughput following the upgrade. (b) Plotting the ratio of the two spectra shows the fourfold increase toward the blue end, whereas the red end is ~45% better.

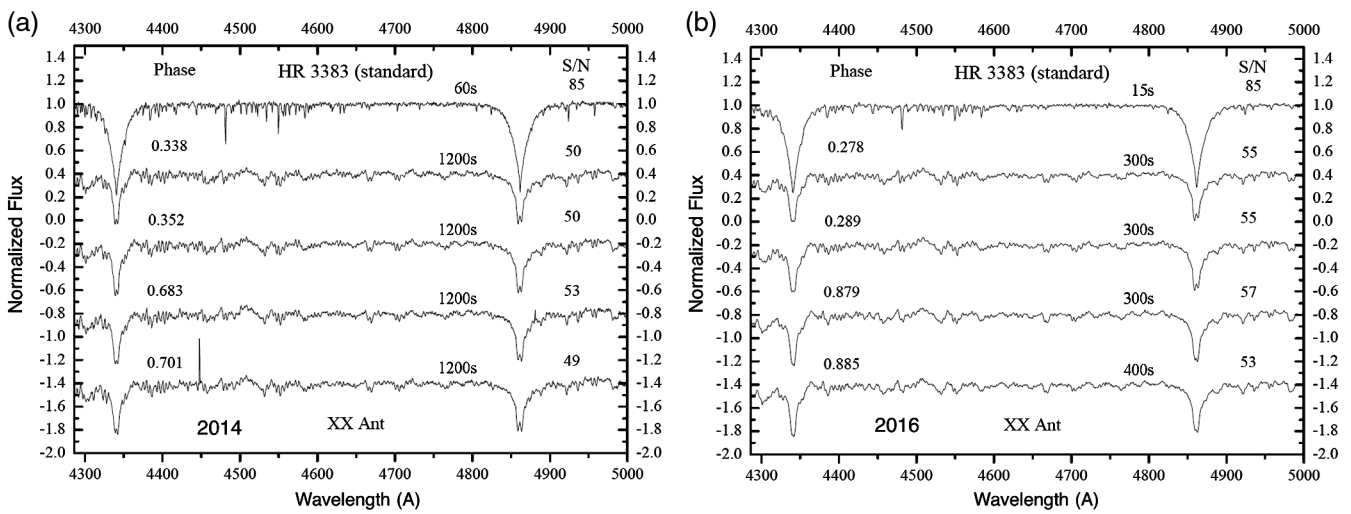

Fig. 10 These two panels show the same standard star (HR3383) and four spectra of the same Algol target (XX Ant) at various orbital phases, (a) as observed with Cassie in 2014 and (b) with SpUpNIC in 2016. Despite the 2014 exposures being four times longer, the S/N (indicated near the red end) is still higher in the SpUpNIC spectra.

Several thousand potential targets have been identified from reduced proper motion surveys[6] and up to ~50% of WDs exhibit low-level variability.[7] This variability is assumed to be due to rotational effects or the presence of a short-period companion. The Kepler 2 mission, and now the TESS space mission, are yielding photometry of a significant fraction of potential WDs (especially those brighter than magnitude 16) and thus will provide an opportunity to survey a much larger number of WDs. SpUpNIC is able to classify and search for evidence of magnetic fields and metal contamination to help determine the cause of the observed variability in these objects. In excellent conditions (seeing <1"), the blue sensitivity of the instrument allows for WD targets brighter than 17.6 to be classified. Figure 11 shows the spectrum of a newly identified $g' = 17.1$ WD

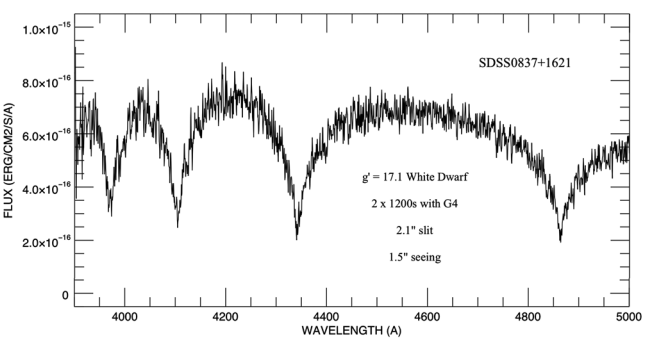

Fig. 11 A new $g' = 17.1$ WD (SDSS0837 + 1621) identified from two 21-min exposures taken with G4 using a 2.1" slit in 1.5" seeing.

(SDSS0837 + 1621) observed in campaign 5 of the Kepler 2 mission. The spectrum consists of two 1200-s exposures taken with G4 in clear conditions with ~1.5" seeing, using a slit width of 2.1″. The spectra were reduced in PyRAF using standard techniques.[8] The broad Balmer lines clearly show that the target is a WD, and initial analysis suggests a temperature of 17905 ± 741 K and a log (g) of 7.001 ± 0.162.

While much of the work done with SpUpNIC to date has been of a stellar nature, the low-resolution G7 is suitable for extragalactic work. A program that involves monitoring various active galactic nuclei has benefitted from the substantially higher throughput of the upgraded spectrograph, particularly toward the blue end of the spectrum. However, the two sources observed in both 1999 and 2016 have clearly decreased in luminosity in recent years, so the performance gain could only be demonstrated with S/N comparisons.

Another ongoing extragalactic project involves gathering spectra for an all-sky redshift survey containing ~45,000 galaxies drawn from the 2MASS extended source catalog with $Ks < 11.75$.[9] The goal of the survey is to study the local density field (out to $D \sim 200$ Mpc) and its effects on the peculiar velocities of galaxies. Obtaining a complete redshift sample as close as possible to the Galactic plane ($|b| = 5$ deg outside of the bulge) is crucial since that area of the sky contains some of the largest concentrations of mass in the local Universe, such as the core of the Great Attractor and the Pisces-Perseus supercluster. Redshifts are measured by means of cross-correlation with absorption-line templates. To obtain $\sigma(cz)$, ~50 km/s requires about 300 counts in the continuum around 6000 Å. Under clear conditions, SpUpNIC achieves the required signal within 5 min, whereas the old spectrograph took 15 min. The increased instrument throughput thus directly leads to increased observing efficiency. Figure 12 shows a map of 300 galaxies in this program that were observed with SpUpNIC over a 2-week period.

4.2 *Wavelength Ranges and Resolutions*

Observations of the recurrent nova RS Oph are used to illustrate (in Fig. 13) the increase in wavelength range due to SpUpNIC's faster camera optics and slightly wider CCD (2048 pixels, compared to 1798 for the SpCCD). G5 spectra of the region around $H\alpha$ were obtained with the old spectrograph in May 2012[10] and with SpUpNIC, in September 2016, in monitoring variability

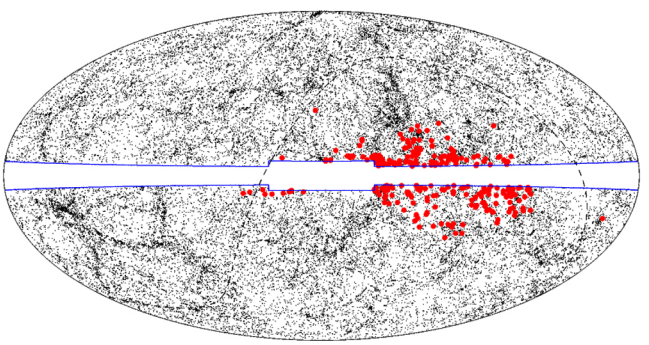

Fig. 12 Aitoff plot in Galactic co-ordinates showing the 300 galaxies in the main survey that were observed with SpUpNIC during two weeks of 1.9-m time. During these runs, redshifts were also obtained for a further 100 targets belonging to an extended sample (not plotted here). The central strip is the zone of avoidance, the densest part of the Milky Way, which is heavily obscured by dust.

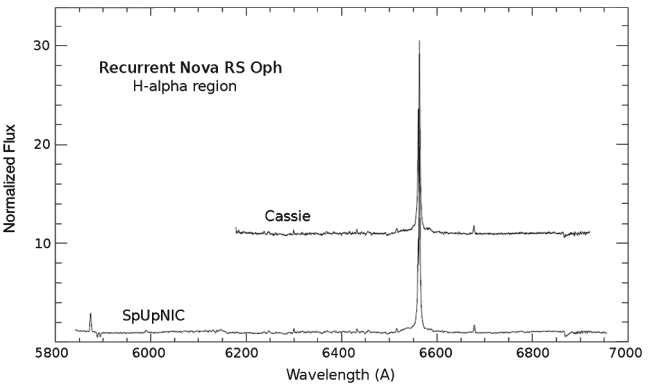

Fig. 13 Spectra of the $H\alpha$ region of the recurrent nova RS Oph obtained with Cassie in 2012 (arbitrarily shifted for display purposes) and with SpUpNIC in 2016 to illustrate the change in wavelength range due to the new optics and wider CCD.

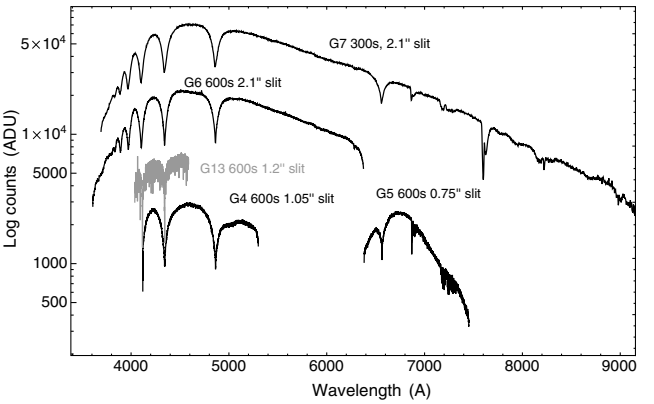

Fig. 14 The spectral coverage in the visible range provided by frequently used gratings. Spectra of EG21, a $V = 11.4$ DA3 spectrophotometric standard, obtained with G4, G5, G6, and G7, are shown black, and a G13 spectrum of the $V = 10.4$ A0 star CD −32°9927 is shown in grey. Exposure times and slit widths were chosen based on the seeing.

in the system's broad, double-peaked $H\alpha$ emission feature. Although the same exposure time of 120 s was used in both cases, the object is variable and a wider slit was used in 2016 due to poorer seeing.

Figure 14 gives an indication of the comparative wavelength coverage provided by a single grating angle for each of the most popular gratings used in the visible range. The spectrophotometric standard EG 21 (a $V = 11.4$ DA3 WD) was observed with G4, G5, G6, and G7. Spectra of a different standard (the $V = 10.4$ A0 dwarf CD −32°9927) were obtained while testing the new, higher-resolution G13, as EG 21 was not visible at the time. Note that the full wavelength range available for each grating is much broader than indicated in Fig. 14, due to the grating angle being adjustable. Figure 15 shows the complete range that can be observed with G13, obtained using four different grating angle settings.

G13 was purchased specifically to enable the study of magnetic activity levels of late-type main sequence stars hosting extrasolar planets. There is evidence that the activity levels of these stars can affect the physical and atmospheric properties of close-in giant planets,[11,12] but currently available data are insufficient to provide a definitive answer.[13]

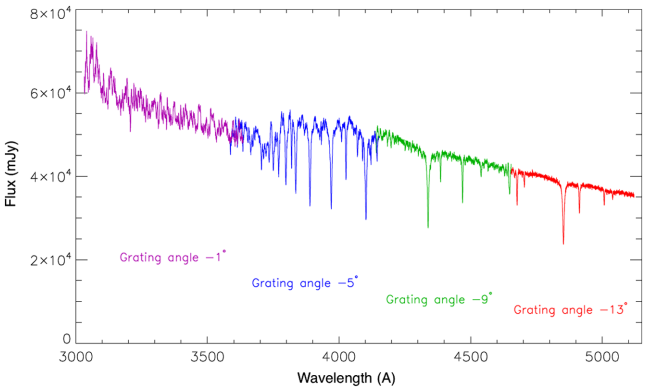

Fig. 15 Flux-calibrated spectrum of the $V = 5.2$ O9.5V standard star HR 1996 obtained with G13, using the four different grating angles indicated.

Magnetic activity heats the chromospheres of stars, causing emission peaks to form in the centers of some spectral lines. For F, G, and K dwarfs, the magnetic activity can be investigated via chromospheric emission in the calcium H and K lines at 3933.67 and 3968.47 Å.[14,15] These measurements can be made spectroscopically using the ratios of fluxes in passbands 1.1 Å wide centred on the H and K lines, relative to two continuum passbands centred on 3901 and 4001 Å.[16] G13 was selected to have a high throughput in this spectral region and sufficient dispersion to yield a spectral resolution of ~1.0 Å. Example spectra are plotted in Fig. 16, where the emission in the centers of the H and K lines is particularly obvious for GJ 9827 (a K6 V star).

SpUpNIC's near-infrared performance (from ~7000 to 10,000 Å) is demonstrated by observations of about two dozen symbiotic stars and several M-type giant standard stars made with G11 during two week-long observing runs in 2016 and 2017 (see Table 4 for a journal of the observations for selected objects). A grating angle of ~5.8 deg yielded low-resolution spectra of the 7200–9600 Å range, which includes the calcium triplet that serves as a useful diagnostic for stellar luminosity, metallicity, and activity. Sample spectra are shown in Fig. 17.

4.3 *Radial Velocity Precision*

W Ursae Majoris-type variables are eclipsing contact (EC) binary stars with orbital periods of less than a day and mass ratios between 0.08 and 0.8.[17] Their short orbital periods pose

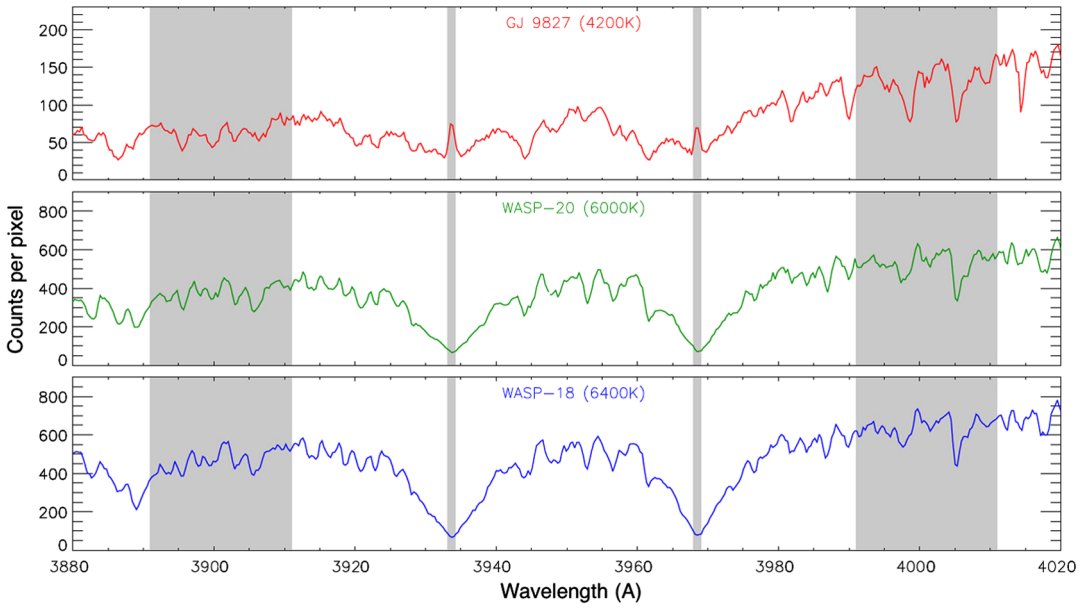

Fig. 16 G13 spectra of three late-type (F, G, and K) dwarfs that host transiting planets. The names and effective temperatures of the stars are labeled on the plots and the gray regions mark the passbands used to calculate the amount of flux produced in the centers of the calcium H and K emission lines.

Table 4 Observational parameters for targets to demonstrate near-infrared performance.

	V	*I*	*J*	Date	Exposures		Slit width		Conditions
Object	Mag	Mag	Mag	UT-middle	No.*exp time (s)	Airmass	Arc sec	S/N	Seeing/Hum./$T - T_{dev}/T_{DOME}$/Sky
LMC N19	16.4	14.3	12.7	October 25, 2017, 00:15:12	5*600	~1.25	1.50	~20–30	~0.9′/29%/~18/13.5°C/clear
CD-27° 8661	10.2		5.3	March 21, 2016, 00:31:54	21*10	~1.06	1.80	~50–80	Poor/80%/~3/7°C/clear
HR 1264	4.5	1.4	0.6	March 22, 2016 19:07:19	27*1.2	~1.61	1.50	>100	~1.7′/52%/~10/13°C/clear

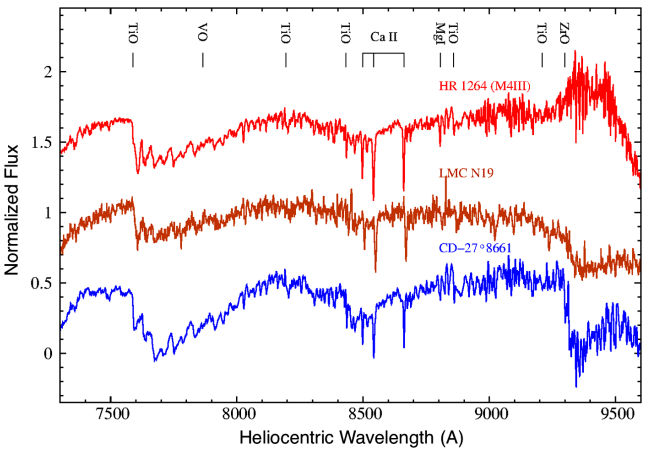

Fig. 17 Spectrum of the symbiotic star LMC N19, compared with spectra of a well-known S-type star (CD-27°8661) that contains a s-process-enhanced red giant, and HR 1264 (=HD 25705) - a M4 type giant spectroscopic standard. For clarity, the normalized spectra of CD-27° 8661 and HR 1264 are shifted by −0.6 and +0.6, respectively.

an observational challenge, as spectroscopic exposures need to be shorter than 1%–2% of the orbital period in order to minimize spectral line blurring due to radial velocity (RV) changes. Numerous symmetric, narrow Fe I, Fe II, and other "metal" lines in the 4000–4500 Å region are accessible with the 1200 lines/mm G4 and are well suited to cross-correlation techniques for measuring radial velocities. While the old spectrograph yielded velocities for $V < 11$ EC binary targets, SpUpNIC achieves sufficient S/N in the time available for a $V = 13$ object with an orbital period of 0.314 days. The resulting RV curve is shown in the left-hand panel of Fig. 18.

The right-hand panel in Fig. 18 shows the RV curve determined for a known $V = 16$ cataclysmic variable with $H\alpha$ emission and an obvious late-type component. A total of 28 spectra (each 600–900s long) were taken with G6 and cross-correlated with the 5000–6500 Å region of a late type spectrum. The resulting RV curve has a period of slightly over 6 h (determined from the spectra). CuAr arcs were taken every 40 min, which was sufficient to model shifts due to flexure at this resolution. The resulting velocities fit the best sine curve with an RMS scatter of 17 km/s and the velocity semiamplitude is 271 km/s, so the S/N is excellent. The data were obtained the day before the full moon and the seeing was ordinary, so the 17 km/s scatter largely reflects the S/N of the individual spectra. The estimated errors in the cross-correlation velocity were similar in magnitude.

5 Technical Issues

5.1 *Grating Stability*

The SpUpNIC grating mechanism initially proved problematic, due to a variety of mechanical instabilities. A series of interventions addressed the different issues and sufficiently improved the performance of this critical assembly. The list of changes included: adapting the PLC software to always drive the grating motor in the same direction when setting the angle (so as to eliminate backlash), replacing the key on the output shaft of the gearbox to ensure a tighter fit in the keyway (thus significantly reducing play), adding a pneumatically actuated disk-brake to lock the grating frame in place once the desired angle has been set (thus eliminating any remaining play in the motor and gearbox), and, finally, adding lateral braces to support the cantilevered grating-holder frame and thus prevent "diving-board" deflections resulting from pointing the telescope around the sky.

The subtle signature of this pernicious final problem is worth elaborating on. Arc spectra were taken with the telescope at zenith, before pointing in different directions and taking more arcs. As anticipated, the arc lines were seen to shift when pointing around the sky, but the all-important clue was the fact that the lines shifted in the same direction, regardless of which way the telescope was tilted. This can only be explained by the fact that having the telescope vertical subjects the grating-holder frame to the maximum gravity-vector and, hence, deflection. Any deviation from vertical results in a smaller component of this force, and so, the lines are shifted less when pointing anywhere else. The extent of the improvement due to the final set of changes is shown in Fig. 19, which plots the shift of a particular arc line (in pixels) as a function of telescope azimuth prior to the fix (upper panel) and after the addition of the mechanical braces (lower panel).

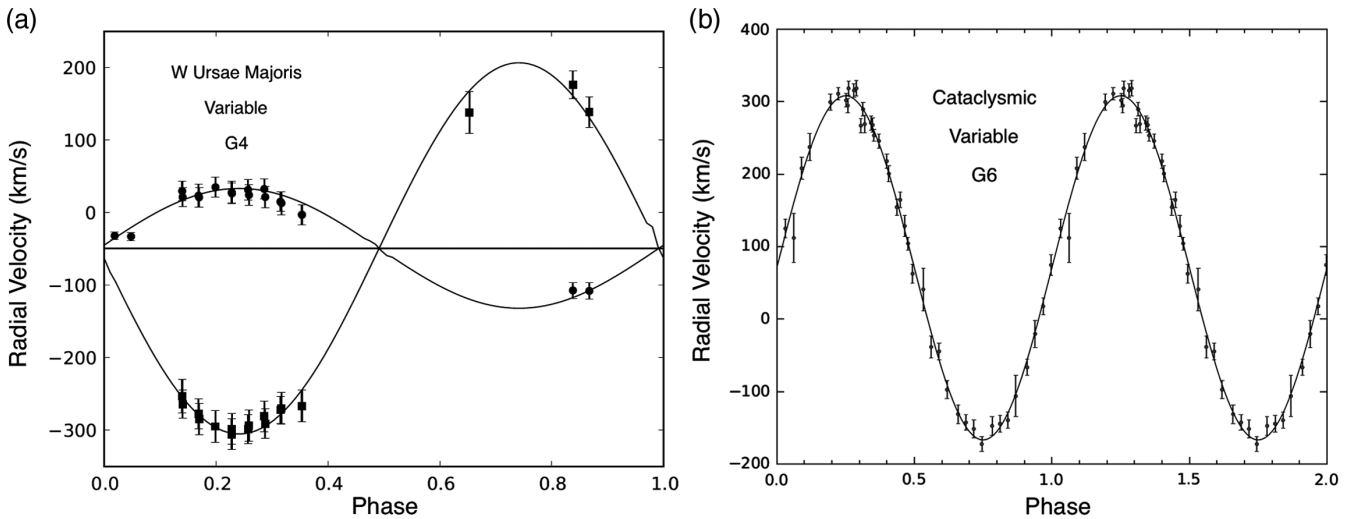

Fig. 18 (a) RV curves obtained with G4 for the $V = 13$ EC binary ASAS 002449-2744.3 and (b) using G6 for a $V = 16$ cataclysmic variable.

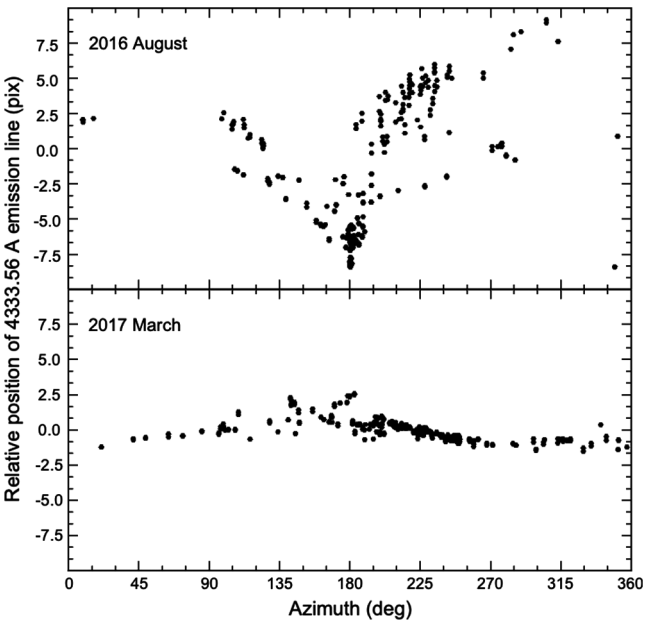

Fig. 19 The instability of the original grating mechanism resulted in large shifts when pointing around the sky (top). The introduction of additional braces to stabilize the grating-holder frame against "diving-board" deflections in late 2016 improved the stability considerably (bottom).

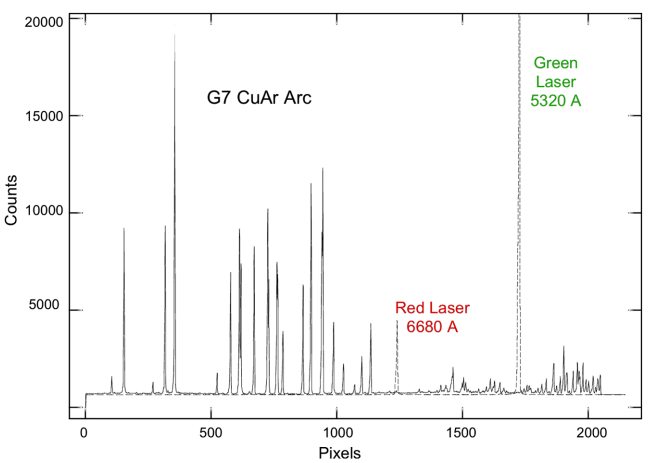

Fig. 20 Red (6680 Å) and green (5320 Å) laser light injected into the spectrograph (dashed), shown along with a low-resolution CuAr arc spectrum (solid), taken with the 300 lines/mm G7.

5.2 *Image Quality*

The line spread functions for data taken with the low-resolution gratings (particularly noticeable in G7 and G12 spectra) deviate from Gaussian profiles, showing a distinct asymmetry. The blue side of a line is steeper than a Gaussian, whereas the red side includes a faint extension. Since arc lines may be blended at such low resolutions, we manually injected red and green laser light into the spectrograph to avoid having the source contribute to the line shape while exploring this effect. Spectra were then taken with the commonly used low- and high-resolution gratings, G7 and G4, respectively. The G4 wavelength range only includes the green laser (at 5320 Å), but the 6680 Å red line appears along with the green one in G7 spectra (see Fig. 20).

Observed with G4, the green 5320 Å laser line is well approximated by a Gaussian profile for all but the lowest intensity levels, where the line wings are broader and very slightly asymmetrical [see Fig. 21(a)]. With G7, however, the laser lines are clearly distorted, and so, FWHM and velocity measurements may be compromised. This has not been an issue since G7 tends to be used for spectral classification and redshift measurements, but users are advised of this effect.

6 Summary

The Cassegrain spectrograph on the SAAO 1.9-m telescope has been extensively upgraded, providing the local and international user community with a considerably more efficient and user-friendly low- to medium-resolution spectrograph. Observers can select any of the 10 surface-relief diffraction gratings for the duration of their run, or manually change gratings during the course of a night if necessary. This grating suite offers a variety of wavelength-range and resolution combinations that span the full optical domain (from ~3300 Å) and extend into the near-infrared (out to ~1 μm), with resolving powers ranging between roughly 500 and 6500. The instrument thus accommodates a broad array of galactic and extragalactic research interests, several examples of which have been presented here in describing the performance of the instrument.

The most significant enhancements to the spectrograph include:

- A throughput increase that ranges from 45% to 400% (from red to blue)
- Broader wavelength coverage, both overall (~3300–10,000 Å) and per grating

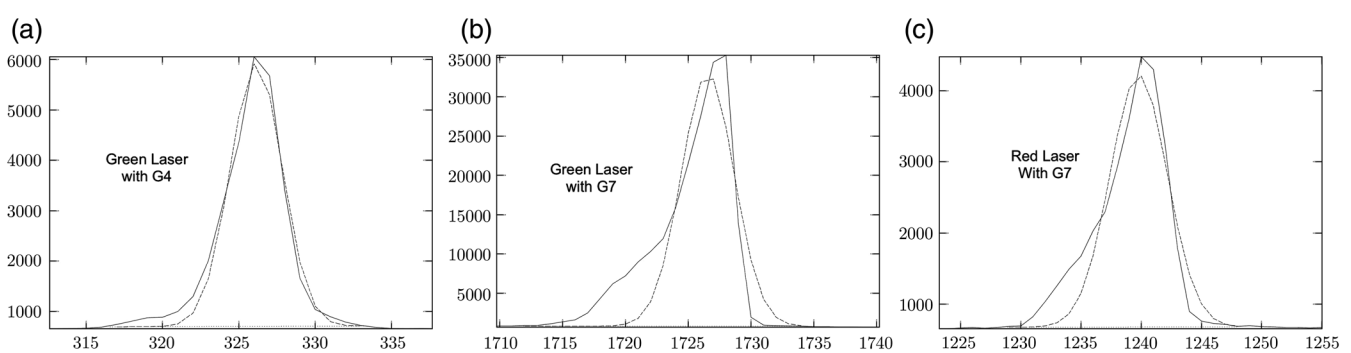

Fig. 21 Gaussian fits (dashed) to laser lines as observed (a) with the high-resolution G4 and (b) and (c) the low-resolution G7. The green laser line observed with G4 is well approximated by a Gaussian, but the line asymmetries are clearly shown in (b) and (c) for the green and red lines, respectively, observed with the low-resolution G7.

Table 5 SpUpNIC characteristics.

Parameter	Specification
Detector	E2V CCD42-10 1024 × 512 pixels (frame-transfer mask blocks 256 rows)
CCD temperature	−105°C (168 K)
Field-of-view	Slit length 2 arc min
Saturation	65,536 ADU
Linearity	<50,000 ADU
Faint/slow mode[a]	1.15 e^-/ADU gain; 2.57 e^- read noise; 4.1-s readout[b]
Bright/fast mode	5.55 e^-/ADU gain; 6.68 e^- read noise; 2.4-s readout[b]
Faint/fast mode	2.06 e^-/ADU gain; 15.8 e^- read noise; 2.4-s readout[b]
Bright/slow mode	2.80 e^-/ADU gain; 2.53 e^- read noise; 4.1-s readout[b]
Total wavelength range	3300–10,000 Å
Resolving power	500–6500
Limiting magnitude	$V \sim 18$ with lowest resolution grating (G7) in 1800 s

[a]Most common setting.
[b]Readout times are given for 1 × 2 binning, times are approximately double for 1 × 1.

- A more modern (higher efficiency) CCD that reads out in just 4 s
- A rear-of-slit viewing system that streamlines the acquisition process
- Full software control of all mechanisms within the instrument via a user-friendly GUI
- A quick-look pipeline that produces and displays wavelength-calibrated spectra seconds after readout
- A ∼2200 lines/mm grating blazed at 5000 Å, where the new CCD's efficiency peaks

Key features of the new system are summarized in Table 5.

SpUpNIC is typically scheduled for four out of every five weeks, and roughly half of that time involves students, including undergraduates majoring in astronomy who learn how to observe with the instrument and then reduce the resulting data.

The spectra shown here, and in Ref. 2, give indications of exposure times and resulting S/N for a selection of objects. Future work will include the development of an exposure-time calculator for the spectrograph.

Acknowledgments

This paper uses observations made at the South African Astronomical Observatory, which is supported by the National Research Foundation (NRF) of South Africa. We acknowledge financial assistance from the Leverhulme Trust, in the form of a Philip Leverhulme Prize, which supported JS and enabled the purchase of G13. CG and DP have been financially supported by a Polish National Science Centre grant SONATA No. DEC 2015/19/D/ST9/02974. We gratefully acknowledge John Booth's invaluable mechanical engineering insights that helped us to resolve many a tricky problem on this instrument. Close colleagues and friends of the remarkable Darragh O'Donoghue will forever wish that he was still with us and able to enjoy observing with the spectrograph's wonderful new camera optics that he designed many years ago.

References

1. I. S. Glass, "The story of the Radcliffe telescope," *Q. J. R. Astron. Soc.* **30**, 33–58 (1989).
2. L. A. Crause et al., "SpUpNIC (Spectrograph upgrade: newly improved Cassegrain) on the South African Astronomical Observatory's 74-inch Telescope," *Proc. SPIE* **9908**, 990827 (2016).
3. R. S. Stobie et al., "The Edinburgh-Cape blue object survey," *MNRAS* **287**, 848–866 (1997).
4. D. Tody, "IRAF in the nineties" in *Astronomical Data Analysis Software and Systems II*, A.S.P. Conference Series, R. J. Hanisch, R. J. V. Brissenden, and J. Barnes, Eds., Vol. **52**, p. 173, Astronomical Society of the Pacific, San Francisco (1993).
5. S. J. Kleinman et al., "SDSS DR7 white dwarf catalog," *Astrophys. J. Suppl. Ser.* **204**(1), 5 (2013).
6. G. Fusillo et al., "A catalogue of white dwarf candidates in VST ATLAS," *MNRAS* **469**, 621–629 (2017).
7. D. Maoz, T. Mazeh, and A. McQuillan, "Kepler and the seven dwarfs: detection of low-level day-time-scale periodic photometric variations in white dwarfs," *MNRAS* **447**, 1749–1760 (2015).
8. P. D. Dobbie et al. "New Praesepe white dwarfs and the initial mass-final mass relation," *MNRAS* **369**, 383–389 (2006).
9. J. P. Huchra et al., "The 2MASS Redshift survey– description and data release," *Astrophys. J. Suppl. Ser.* **199**(2), 26 (2012).
10. H. L. Worters and M. T. Rushton, "Fast Hα emission line variability in RS Ophiuchi," *MNRAS* **442**(3), 2637–2640 (2014).
11. H. A. Knutson, A. W. Howard, and H. Isaacson, "A correlation between stellar activity and hot jupiter emission spectra," *Astrophys. J.* **720**, 1569–1576.
12. J. D. Hartman, "A correlation between stellar activity and the surface gravity of hot Jupiters," *Astrophys. J. Lett.* **717**(2), L138–L142 (2010).
13. P. Figueira et al., "Revisiting the correlation between stellar activity and planetary surface gravity," *A&A* **572**, A51 (2014).
14. A. H. Vaughan, G. W. Preston, and O. C. Wilson, "Flux measurements of CA II H and K emission," *Publ. Astron. Soc. Pac.* **90**, 267–274 (1978).
15. R.W. Noyes et al. "Rotation, convection, and magnetic activity in lower main-sequence stars," *Astrophys. J.* **279**, 763–777 (1984).
16. H. Isaacson and D. Fischer, "Chromospheric activity and jitter measurements for 2630 stars on the California Planet Search," *Astrophys. J.* **725**, 875–885 (2010).
17. R. W. Hilditch, *An Introduction to Close Binary Stars*, Cambridge University Press, Cambridge (2001).

Biographies of the authors are not available.